Optical Lattice Trapping of ^{199}Hg and Determination of the Magic Wavelength for the Ultraviolet $^1S_0 \leftrightarrow {}^3P_0$ Clock Transition

L. Yi, S. Mejri, J. J. McFerran,[†] Y. Le Coq, and S. Bize[*]

LNE-SYRTE, Observatoire de Paris, 61 Avenue de l'Observatoire, 75014 Paris, France

(Received 30 November 2010; published 18 February 2011)

We report on the Lamb-Dicke spectroscopy of the doubly forbidden $(6s^2)^1S_0 \leftrightarrow (6s6p)^3P_0$ transition in ^{199}Hg atoms confined to a vertical 1D optical lattice. With lattice trapping of $\lesssim 10^3$ atoms and a 265.6 nm probe laser linked to the LNE-SYRTE primary frequency reference we have determined the center frequency of the transition for a range of lattice wavelengths and at two lattice trap depths. We find the Stark-free (magic) wavelength to be 362.53(0.21) nm—essential knowledge for future use of this line in a clock with anticipated 10^{-18} range accuracy. We also present evidence of the laser excitation of a Wannier-Stark ladder of states in a lattice of well depth $10E_R$.

DOI: 10.1103/PhysRevLett.106.073005 PACS numbers: 32.30.Jc, 32.10.Dk, 37.10.Jk, 42.62.Fi

Through the comparison of many exceptionally accurate frequency standards, tighter constraints can be placed on the possible present-day variation of fundamental constants [1–4]. This gives stimulus for increasing the number of atomic clocks based on different quantum absorbers with fractional frequency accuracies in the 10^{-17}–10^{-18} range. Such high-performance frequency references can be applied to other tests of relativity [5,6], as well as gravitational mapping through redshift measurements [7]. We are now in the epoch when the accuracy of the best optical clocks surpasses that of microwave primary standards. Most notable at present are the aluminum ion [8], mercury ion [9], strontium lattice [10–12], and ytterbium lattice clocks [13,14]. While the lowest uncertainty for ultranarrow transition frequencies is presently exhibited by ion clocks, optical lattice clocks are relatively new in their development and have already surpassed the accuracies of conventional neutral cold-atom clocks [11]. Because of the presence of a larger number of quantum absorbers compared with their ionic counterparts, in principle, it should be possible to evaluate frequency shifts and uncertainties more rapidly. The anticipated minimum uncertainty for such (red-detuned) lattice clocks is in the 10^{-18} range [15,16].

Lattice clocks have been under development since the proposal to constrain neutral atoms in an optical lattice while probing the ultrafine transition [17]. Well-advanced lattice clocks use Sr [11,18,19] and Yb [13,14]. The present fractional uncertainties for these standards are in the low 10^{-16} range, both of which are dominated by the blackbody radiation shift. Favorable to a Hg-based clock is the lower atomic polarizability of Hg, which implies that the shift due to blackbody radiation is more than an order of magnitude lower. However, spectroscopy with ultracold Hg is challenging: only recently has cooling and magneto-optic trapping of Hg atoms been demonstrated [15,20,21]. Applied more broadly, ultracold Hg is a promising candidate for entangled atom experiments and photo-association spectroscopy in Hg_2 molecular studies [22,23].

Optical lattice trapping constrains atoms to a subwavelength region, permitting recoil-free spectroscopy with resolved motional sidebands [24]. However, since the light used to produce the lattice of potentials causes a deliberate (spatially dependent) shift of the energy levels, it is necessary to find a wavelength at which both the upper and lower clock states change by equal amounts, i.e., the Stark-free (magic) wavelength, λ_m [17]. In the case of the $^1S_0 \leftrightarrow {}^3P_0$ Hg line, theoretical calculations estimate this wavelength to be $\sim$363 nm [15,25]. Here we perform Lamb-Dicke spectroscopy on this line for ^{199}Hg atoms confined in a dipole lattice trap. By repeating frequency measurements at a range of lattice wavelengths and at two different lattice depths, we infer λ_m. The carrier spectrum exhibits asymmetry away from this light-shift free wavelength; this characteristic is used to infer the magic wavelength by a second means. The two methods show very good agreement. This is the first demonstration of lattice-bound atomic spectroscopy in the deep ultraviolet to our knowledge.

The overall experimental arrangement is shown in Fig. 1 and the relevant energy levels are shown in Fig. 2(a). There are two frequency quadrupling sequences: (i) for the cooling light at 253.7 nm and (ii) for the $^1S_0 \leftrightarrow {}^3P_0$ probe at 265.6 nm. There is also a separate frequency doubling stage followed by a power enhancement cavity for the lattice light. Stabilization of the cooling light is performed with saturated absorption in a Hg vapor cell. Stabilization of the clock probe relies on a 8.5×10^5 finesse ultrastable optical cavity heavily shielded from the environment. A fiber laser at 1062 nm locked to this cavity forms the ultrastable light source (USL) from which the 265.6 nm probe is derived [26]. A phase link is made between the infrared USL and the LNE-SYRTE primary frequency reference [20,26]. The USL has demonstrated a fractional frequency instability of 5.6×10^{-16} [27] and during the course of the measurements here the drift rate remained below 50 mHz s^{-1}.

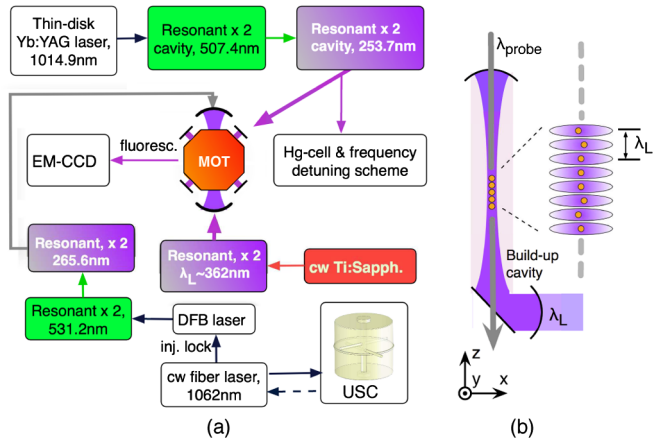

FIG. 1 (color online). (a) Schematic of the experiment. MOT, magneto-optical trap; EM, electron multiplication; DFB, distributed feedback (semiconductor); USC, ultrastable cavity. (b) A representation of atoms distributed vertically at nodes of the E-light field maxima.

The vacuum apparatus and magneto-optical trap (MOT) configuration is described in previous reports [20,21]. We briefly point out that the cooling is carried out with the 1.3 MHz wide $^1S_0 \leftrightarrow {}^3P_1$ transition at 253.7 nm with an intensity of $\sim$700 Wm^{-2} at the MOT center. A tunable CW Ti:sapphire laser delivering 900 mW is the source laser for producing the lattice light. Its light is frequency doubled by use of a Brewster cut LiB_3O_5 crystal in a bow-tie resonant cavity with the Hänsch-Couillaud locking scheme. Up to 280 mW of UV light is produced at a wavelength near 363 nm. An optical cavity, resonant with the 363 nm light, is maintained under vacuum in conjunction with the MOT chamber. The cavity is aligned vertically and the 363 nm reflecting optics allow passage for the probe light at 265.6 nm. A 45° planar mirror, set internal to the cavity below the MOT, is designed to remove polarization degeneracy. The cavity design is free of windows, helping to permit a high build up factor and

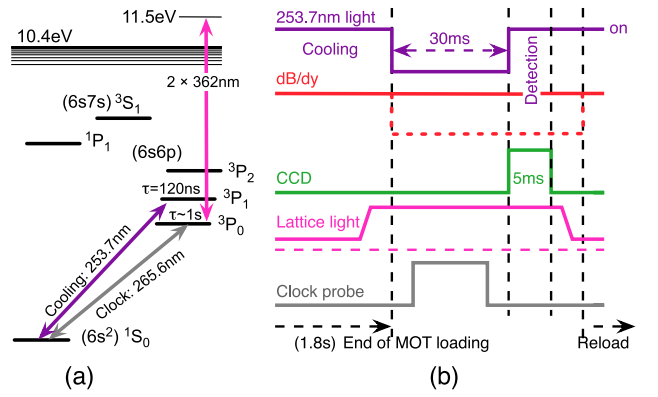

FIG. 2 (color online). (a) Relevant energy levels for neutral mercury (hyperfine structure for the fermions is omitted). Repumping with the $^3S_1$ level is not employed. (b) Operating sequence for spectroscopy. For atom detection, only two of the cooling beams are re-engaged.

reducing the level of the scattered light reaching the detection system. Based on the internal circulating power, P, of the cavity we can estimate the potential depth of the lattice trap from, $U_0 = 4\alpha_{\mathrm{Hg}}(\lambda_L)P/(\pi c \epsilon_0 w_b^2)$, where $\alpha_{\mathrm{Hg}}(\lambda_L)$ is the ground-state ac atomic polarizability ($\sim 5.3 \times 10^{-40}$ m^3), ϵ_0 is the permittivity of free space, and w_b is the waist radius—here equal to 120 μm. A suitable energy scale for describing the potential of the lattice trap is the recoil energy, $E_R = h^2/(2m\lambda_L^2)$, imparted to an atom of mass m by a lattice photon with wavelength λ_L. The corresponding temperature is $E_R/k_B = 365$ nK. Using a parabolic approximation for the potential at the bottom of the trap, the longitudinal trap frequency is: $f_z = 2\pi\hbar\sqrt{U_0/E_R}/(m\lambda_L^2)$ with radial frequency: $f_r = f_z\lambda_L/(\sqrt{2}\pi w_b)$. Owing to coating damage to the lattice cavity optics caused by the circulating 363 nm light under vacuum, the power was limited to 3 W. The corresponding potential depth is $10E_R$ with $f_z = 50$ kHz. The vertical alignment of the lattice cavity removes the degeneracy between vibrational states of adjacent potential wells (forming the Wannier-Stark ladder of states) and therefore inhibits tunneling between sites [28]. However, transitions between these Wannier-Stark states are not expected to be completely suppressed when atoms are distributed across excited axial and transverse motional states of a shallow trap (see below).

The control sequence is illustrated in Fig. 2(b). Atoms are loaded in the MOT for 1.8 s then, after a 10 ms cooling and compression phase, the MOT light field is halted (the magnetic field gradient is maintained). The atoms sufficiently cold remain confined in the wells of the lattice. The lattice light is held at its maximum level for only a short duration to minimize damage to the cavity mirrors. While trapped, the atoms are probed with $\sim$200 μW of 265.6 nm light for 20 ms. The typical release period is 30 ms before ground-state detection with the 254 nm light (the trap lifetime is $\sim$200 ms). For the 5 ms detection period only two MOT beam pairs are used; the horizontal beam remains blocked to reduce stray light reaching the CCD. As a further consequence, recapturing of atoms during detection is highly unlikely. The fraction of atoms transferred from the MOT to the lattice trap has been calculated based on a waist size of 120 μm for the lattice light (the rms radius of the MOT cloud is $\sim$100 μm). At 3 W and 60 μK we expect 0.07% of the ^{199}Hg atoms to be transferred to the lattice. In the experiment we detect at least 500 atoms, or 0.05% of the initial MOT cloud, while the detection limit is equivalent to $\sim$40 atoms per cycle.

A fiber link in the IR between the USL and the Hg apparatus includes active noise cancellation with a double passed acousto-optic modulator. Sweeping the drive frequency of this modulator performs the scanning of the clock probe frequency. An example of the $^1S_0 \leftrightarrow {}^3P_0$ transition spectrum is shown in Fig. 3(a), where the time to generate the trace was 210 s. The line center and width were determined using Lorentzian line fitting (one may

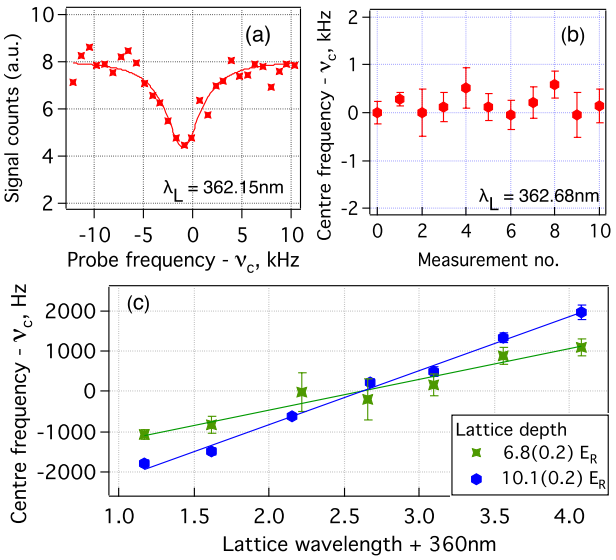

FIG. 3 (color online). (a) Profile of the ^{199}Hg clock transition at a lattice wavelength of 362.15 nm. The fitted line is a Lorentzian profile. $\nu_c = 1\,128\,575\,290\,808\,400$ Hz. (b) A series of center frequency measurements recorded for the same lattice wavelength (362.68 nm) and lattice depth ($10E_R$). (c) Light-shift frequency versus wavelength for two intensity levels of the lattice trap.

expect to use a sinc^2 line shape, but the difference is inconsequential). Frequency measurements and drift rate of the probe light were measured at regular intervals of 6 to 12 h. This enabled the frequency of the probe signal to be determined with close to Hz-level uncertainty at the time of each clock-line scan. The frequency is offset by the value for the ^{199}Hg line reported in [20], i.e., $\nu_c = 1\,128\,575\,290\,808\,400$ Hz. The FWHM linewidth of $\sim$4 kHz is broader than expected; e.g., the Fourier transform width of the probe pulse is $\sim$40 Hz. It is not easily affected by the 265.6 nm intensity or duration; further discussion follows below. There was no measurable frequency shift created by the MOT's field gradient, which was maintained during the probing period to improve the signal strength.

At a given lattice wavelength and lattice depth, spectra such as that of Fig. 3(a) were recorded multiple times and the center frequency deduced for each. A series of such measurements is shown in Fig. 3(b), where $\lambda_L = 362.675(1)$ nm and $U_0 = 10.1(0.2)E_R$ (the error bars follow from the line fitting procedure). From this we determine the weighted mean and 1σ uncertainty for the line center frequency. The process was repeated for a range of lattice wavelengths and at two lattice intensity levels, the results of which are summarized in Fig. 3(c). The light-shift frequency is seen to vary linearly with lattice wavelength and the crossover point corresponds to the Stark-free wavelength, here equal to 362.61(0.21) nm. This is within 0.5 nm (or 0.15%) of a recent theoretical calculation [25]. Reassuringly, the crossover lies within 10 Hz of the frequency previously reported for the ^{199}Hg

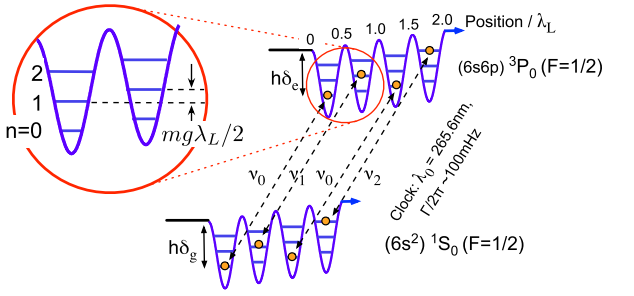

FIG. 4 (color online). Periodic light shifts of the lower and upper states of the clock transition with several vibrational levels represented. The lattice light is at the Stark-free wavelength when $h\delta_g = h\delta_e$. The shift due to gravity between lattice sites is 885 Hz ($\approx 0.018\times$ that of the axial frequency).

line (which had an associated uncertainty of 5.6 kHz). The ratio of the slopes from the line fitting is 0.57, slightly lower than the intensity ratio of 0.67. The absolute value for the slope of the polarizability is 130 $\mathrm{Hz}E_R^{-1}\,\mathrm{nm}^{-1}$, or $5\times10^{-17}\ E_R^{-1}\,\mathrm{GHz}^{-1}$ when normalized by the clock frequency, which suggests that control of the trapping frequency to a few MHz will be sufficient for future Hg clock operation. For comparison, in the cases of Sr and Yb the slope is $\sim4\times10^{-17}\ E_R^{-1}\,\mathrm{GHz}^{-1}$. Based on our measurement of λ_m we find that, from the upper clock state, two photons at λ_m can cause excitation into the continuum with 1.1 eV above the single ionization threshold. This experimental result helps better determine the two-photon ionization rate and hyperpolarizability [15].

Since there is no deliberate additional cooling of the lattice trapped atoms, they will be distributed across vibrational states, as loosely portrayed in Fig. 4. Moving away from λ_m the oscillator trap levels for two clock states become unequal, hence the frequencies $\nu_0, \nu_1, \nu_2, \ldots, \nu_n$ are no longer equal and the overall carrier spectrum becomes a superposition of lines profiles with frequency separation $d\nu_v$ [29]. Assuming a Boltzmann distribution, the occupation probability over the vibrational states is $p_{n+1}/p_n = \exp(-hf_z/k_BT) = f_B$, where T is the temperature. Supporting this are the results shown in Figs. 5(a) and 5(b) recorded for lattice wavelengths of 361.17 and 364.08 nm, respectively. The opposite skew in the asymmetry is clearly seen. The line shape function for fitting to the data is given by,

$$\mathcal{L}(\delta, d\nu_v) \propto -\sum_{n=0}^{N}\left(\frac{(f_B)^n}{(\delta-\nu_0+nd\nu_v)^2+\Delta\nu^2}\right), \quad (1)$$

where δ is the frequency detuning and ν_0 is the center frequency for $n=0$ (ν_0 can be arbitrary here). A constraint is applied to N, since the well depth only permits at most four longitudinal vibrational levels. The linewidth, $\Delta\nu$, is set by that measured near the crossover wavelength (FWHM $= 2\Delta\nu \sim 4.1$ kHz). From the line fitting we extract the Boltzmann factor ($f_B \approx 0.55$) and $d\nu_v$. (Aside, given f_B and knowing the axial frequency to be

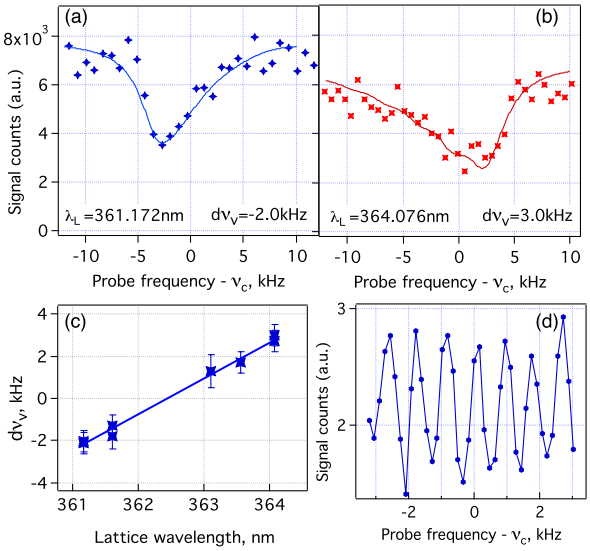

FIG. 5 (color online). Profiles of the ^{199}Hg clock transition displaying asymmetry: (a) $\lambda_L = 361.17$ nm with $d\nu_v = -2.0$ kHz; (b) $\lambda_L = 364.08$ nm with $d\nu_v = 3.0$ kHz. Line-fit profiles are described in the text. (c) Vibrational frequency difference versus lattice wavelength. (d) Higher resolution scan of the ^{199}Hg clock transition near the magic wavelength ($\lambda_L = 362.678$ nm).

$\sim$50 kHz we find $T \approx 4$ μK, which matches the depth of the lattice potentials). By using spectra where the asymmetry is evident we plot $d\nu_v$ as a function of the lattice wavelength, as seen Fig. 5(c). The wavelength at which $d\nu_v = 0$ is 362.44(0.25) nm, in good agreement with the previous result from direct spectroscopy.

When probing the clock transition at $\lambda_L \approx \lambda_m$ and with the MOT gradient field off, in an attempt to obtain a narrow line spectrum, we observe the behavior seen in Fig. 5(d). The periodic pattern is suppressed when the B-field gradient remains on—for reasons not yet well understood. Here the oscillatory peaks have a period of $\sim$880 Hz. Numerous tests have shown that the period is not easily influenced, for example, by changing the 265.6 nm probe intensity or the lattice depth. Four traces recorded over a period of 1 h remain ''in phase'', and when averaged yielded the same period of $\sim$880 Hz. Our conclusion is that these oscillations arise because, in our shallow trap, excited Wannier-Stark states are delocalized over several neighboring lattice sites, making laser excitation through the Wannier-Stark ladder highly possible. The period observed in the spectrum reflects the change of gravitational energy between neighboring sites, i.e., $mg\lambda_L/(2h) =$ 885 Hz (= Bloch frequency) [28]. By comparison, the expected first-order Zeeman splitting is below 50 Hz due to the applied field used to displace the MOT cloud into the lattice waist. Wannier-Stark transitions have previously been observed through parametric excitation [30,31], but as far as we are aware not through pure optical excitation, as is the case here.

To summarize, ultraviolet light spectroscopy has been carried out on lattice trapped ^{199}Hg atoms. The magic wavelength for the clock line in neutral Hg has been determined by use of two alternative methods. Assuming the mean of the two measured values, we find this wavelength to be 362.53(0.21) nm [32].

The authors are grateful for the support from SYRTE technical services. We thank A. Clairon, A. Gérard, M. Lours, A. Luiten, and J. Lodewyck for their input. SYRTE is UMR CNRS 8630 and is associated with the UPMC. This work is partly funded by IFRAF and by CNES. J. M. is gracious for the support from la Ville de Paris.

*sebastien.bize@obspm.fr
†john.mcferran@obspm.fr

[1] V. V. Flambaum and V. A. Dzuba, Can. J. Phys. **87**, 25 (2009).
[2] S. Blatt *et al.*, Phys. Rev. Lett. **100**, 140801 (2008).
[3] E. Peik *et al.*, Phys. Rev. Lett. **93**, 170801 (2004).
[4] S. Bize *et al.*, Phys. Rev. Lett. **90**, 150802 (2003).
[5] C. M. Will, Living Rev. Relativity **9**, 3 (2006).
[6] N. Ashby *et al.*, Phys. Rev. Lett. **98**, 070802 (2007).
[7] C. W. Chou, D. B. Hume, T. Rosenband, and D. J. Wineland, Science **329**, 1630 (2010).
[8] C. W. Chou *et al.*, Phys. Rev. Lett. **104**, 070802 (2010).
[9] T. Rosenband *et al.*, Science **319**, 1808 (2008).
[10] X. Baillard *et al.*, Opt. Lett. **32**, 1812 (2007).
[11] A. Ludlow *et al.*, Science **319**, 1805 (2008).
[12] F.-L. Hong *et al.*, Opt. Lett. **34**, 692 (2009).
[13] Z. Barber *et al.*, Phys. Rev. Lett. **100**, 103002 (2008).
[14] N. D. Lemke *et al.*, Phys. Rev. Lett. **103**, 063001 (2009).
[15] H. Hachisu *et al.*, Phys. Rev. Lett. **100**, 053001 (2008).
[16] A. V. Taichenachev *et al.*, Phys. Rev. Lett. **96**, 083001 (2006).
[17] H. Katori, M. Takamoto, V. G. Pal'chikov, and V. D. Ovsiannikov, Phys. Rev. Lett. **91**, 173005 (2003).
[18] R. Le Targat *et al.*, Phys. Rev. Lett. **97**, 130801 (2006).
[19] M. Takamoto *et al.*, J. Phys. Soc. Jpn. **75**, 104302 (2006).
[20] M. Petersen *et al.*, Phys. Rev. Lett. **101**, 183004 (2008).
[21] J. J. McFerran, L. Yi, S. Mejri, and S. Bize, Opt. Lett. **35**, 3078 (2010).
[22] E. S. Fry, T. Walther, and S. Li, Phys. Rev. A **52**, 4381 (1995).
[23] T. Walther, J. Mod. Opt. **54**, 2523 (2007).
[24] J. C. Bergquist, W. M. Itano, and D. J. Wineland, Phys. Rev. A **36**, 428 (1987).
[25] A. Ye and G. Wang, Phys. Rev. A **78**, 014502 (2008).
[26] S. T. Dawkins *et al.*, Appl. Phys. B **99**, 41 (2009).
[27] J. Millo *et al.*, Phys. Rev. A **79**, 053829 (2009).
[28] P. Lemonde and P. Wolf, Phys. Rev. A **72**, 033409 (2005).
[29] M. Takamoto and H. Katori, Phys. Rev. Lett. **91**, 223001 (2003).
[30] V. Ivanov *et al.*, Phys. Rev. Lett. **100**, 043602 (2008).
[31] S. R. Wilkinson *et al.*, Phys. Rev. Lett. **76**, 4512 (1996).
[32] The two methods may not be fully independent, hence the unreduced uncertainty.